Enhanced mid-infrared transmission through nanoscale metallic coaxial-aperture arrays

Wenjun Fan, Shuang Zhang, K. J. Malloy and S. R. J. Brueck

Center for High Technology Materials, University of New Mexico, Albuquerque, NM 87106, USA
brueck@chtm.unm.edu

Abstract: Using a single interferometric lithography patterning step along with self-aligned pattern-definition techniques, uniform, large-area metallic coaxial arrays with ~ 100-nm toroidal gaps are fabricated. Enhanced (5×) mid-infrared (4 μm) transmission through these sub-wavelength coaxial arrays is observed as compared with that through the same fractional opening area hole arrays as a result of the complex coaxial unit cell. Varying the coaxial dimensions shifts the resonance wavelength and impacts the maximum transmission; design rules are derived. The ability to control the transmission wavelength combined with dramatically enhanced transmission represent a promising path toward nanophotonic applications.

OCIS codes: (050.1220) Apertures; (050.2770) Gratings; (220.4000) Microstructure fabrication; (220.3740) Lithography.

References and links

1. T. W. Ebbesen, H. J. Lezec, H. F. Ghaemi, T. Thio and P. A. Wolff, "Extraordinary optical transmission through sub-wavelength hole arrays," Nature (London) **391,** 667-669 (1998).
2. H.J. Lezec, A. Degiron, E. Devaux, R.A. Linke, L. Martin-Moreno, F.J. Garcia-Vidal and T.W. Ebbesen, "Beaming light from a subwavelength aperture," Science **297**, 820–822 (2002).
3. W. L. Barnes, W. A. Murray, J. Dintinger, E. Devaux and T. W. Ebbesen, "Surface plasmon polaritons and their role in the enhanced transmission of light through periodic arrays of subwavelength holes in a metal film," Phys. Rev. Lett. **92**, 107401 (2004).
4. H. J. Lezec and T. Thio, "Diffracted evanescent wave model for enhanced and suppressed optical transmission through subwavelength hole arrays," Opt. Express **12,** 3629-3651 (2004), http://www.opticsexpress.org/abstract.cfm?URI=OPEX-12-16-3629.
5. A. Degiron and T. W. Ebbesen, "The role of localized surface plasmon modes in the enhanced transmission of periodic subwavelength apertures," J. Opt. A: Pure Appl. Opt. **7**, S90-S96 (2005).
6. H. F. Schouten, N. Kuzmin, G. Dubois, T. D. Visser, G. Gbur, P. F. A. Alkemade, H. Blok, G. W. 't Hooft, D. Lenstra and E. R. Eliel, "Plasmon-Assisted two-slit transmission: Young's experiment revisited," Phys, Rev. Lett. **94**, 053901 (2005)
7. A. Nahata, R. A. Linke, T. Ishi and K. Ohashi, "Enhanced nonlinear optical conversion from a periodically nanostructured metal film," Opt. Lett. **28,** 423-425 (2003).
8. W. L. Barnes, A. Dereux and T. W. Ebbesen, "Surface plasmon subwavelength optics," Nature (London) **424,** 824-830 (2003).
9. F. I. Baida and D. Van Labeke, "Light transmission by subwavelength annular aperture arrays in metallic films," Opt. Commun. **209,** 17-22 (2002).
10. A. Moreau, G. Granet, F. I. Baida and D. Van Labeke, "Light transmission by subwavelength square coaxial aperture arrays in metallic films," Opt. Express **11,** 1131-1136 (2003), http://www.opticsexpress.org/abstract.cfm?URI=OPEX-11-10-1131.
11. W. Fan, S. Zhang, B. Minhas, K. J. Malloy and S. R. J. Brueck, "Enhanced infrared transmission through subwavelength coaxial metallic arrays," Phys. Rev. Lett. **94**, 033902 (2005).
12. A. Krishnan, T. Thio, T. J. Kim, H. J. Lezec, T. W. Ebbesen, P. A. Wolff, J. Pendry, L. Martin-Moreno, F. J. Garcia-Vidal, "Evanescently coupled resonance in surface plasmon enhanced transmission," Opt. Commun. **200,** 1-7 (2001).
13. S. R. J. Brueck, S. H. Zaidi, X. Chen and Z. Zhang, "Interferometric lithography - from periodic arrays to arbitrary patterns," Microelectron. Eng. **42,** 145-148 (1998).
14. C. Genet, M. P. Van Exter and J. P. Woerdman, "Fano-type interpretation of red shifts and red tails in hole array transmission spectra," Opt. Commun. **225**, 331-336 (2003).
15. F. I. Baida, D. Van Labeke, G. Granet, A. Moreau and A. Belkhir, "Origin of the super-enhanced light transmission through a 2-D metallic annular aperture array: a study of photonic bands," Appl. Phys. B **79,** 1-8 (2004).

#7338 - $15.00 USD Received 3 May 2005; revised 27 May 2005; accepted 27 May 2005

16. N. Marcuvitz, *Waveguide handbook*, (New York: McGraw-Hill, 1951).

1. Introduction

Improvements in fabrication capabilities for metallic nanostructures have led to intense interest in a broad range of applications. Subwavelength periodic metallic hole arrays [1] and a single subwavelength aperture surrounded by a concentric periodically corrugated metal film [2] for enhanced optical transmission are two interesting structures. The generally accepted model for the enhanced transmission is coupling to surface-plasma waves at the metal-dielectric interface [3], although an alternate scattering model [4] has been proposed. Recent studies of the effects of localized surface plasmons (SP) [5] and a revisited Young's experiment [6] have shown that the enhanced transmission is a consequence of SP. From the TE and TM polarization angle-dependent data of metallic coaxial arrays presented here, we reconfirm that the surface plasmons are responsible for the enhanced transmission observed in metallic hole arrays, and that with a coaxial aperture rather than a simple hole significantly enhanced transmission can be achieved. The sub-wavelength scale of these structures will lead to applications in photonic circuits and the localization of the light in the apertures provides an electric-field enhancement that can be used to manipulate light-matter interactions and enhance nonlinear phenomena [7,8]. Arrays of coaxial metallic structures, first proposed by Baida *et al*. [9,10], support additional guided electromagnetic modes and have substantially greater transmission and correspondingly larger field enhancements than do simple hole arrays. We have recently confirmed these predictions experimentally at near-IR wavelengths [11]. The complex coaxial unit cell gives additional degrees of freedom for controlling and optimizing the optical response. By using rigorous coupled-wave analysis (RCWA) simulation as design guide to arrange the spectral overlap between the coaxial transmission peak and the SP peak, a 5× enhanced mid-infrared (4 μm) transmission through these sub-wavelength coaxial arrays is realized as compared with that through hole arrays with the same fractional open area.

2. Fabrication

A detailed procedure is presented for fabricating these structures on a high refractive-index semiconductor - GaAs, which generally exhibits much weaker transmission in hole array experiments due to the large impedance mismatch [12] between the substrate and the incident medium (air). We also demonstrate the scaling of these structures to longer wavelengths, of interest because of applications within the 3- to 5-μm infrared atmospheric-transmission window. We used a process based on interferometric lithography [13] (IL) to fabricate the annular coaxial metal grids. Unlike the more common electron- and ion-beam lithography approaches, for which the throughput is generally low; there is no difficulty in extending the sample area for IL - a parallel optical process that is ideal for making large-areas of periodic structures. All the samples reported here were uniformly fabricated over 1.5×1.5 cm^2 areas on double-polished, semi-insulating GaAs substrates using a self-aligned process requiring only a single lithography step.

Figure 1 illustrates the process flow. 1) The GaAs substrate is first covered with a ~ 400-nm thick blanket sacrificial layer of SiN_x using plasma-enhanced chemical-vapor deposition (PECVD). Next, a 20-nm thick layer of PMMA was applied by spinning, this layer will serve as a sacrificial lift-off dissolution layer in a later processing step. A bottom anti-reflection coating (BARC) layer for i-line lithography was then spun on to minimize reflection of the IL beams from the underlying film stack. Finally, a 500-nm thick positive-tone photoresist (Shipley SPR505A) was applied. 2) IL at a wavelength of 355 nm, 3rd harmonic of a YAG:Nd^{3+} laser, was used to produce periodic post patterns (1.12-μm pitch for all samples discussed herein) in the photoresist (PR). The angle between the two beams determines the period of the pattern, while the exposure flux, post-exposure bake and development parameters control the final pattern line widths. For these square 2D arrays, a second IL

#7338 - $15.00 USD Received 3 May 2005; revised 27 May 2005; accepted 27 May 2005

exposure was applied after a 90° rotation of the sample. 3) A 60-nm thick layer of Cr was deposited on the developed sample. After lift-off, the remaining Cr, a connected film perforated with a 2D array of holes, formed a metal etch-mask on top of the BARC layer. With this robust mask, the pattern was transferred without any change in transverse dimensions through all of the etching processes in steps 4 and 5. 4) An O_2 plasma reactive-ion etch was used to anisotropically etch through the BARC and PMMA layers, followed by anisotropic etching through the SiN_x to generate the locations for the central Au dots of the coaxial array on the substrate surface. 5) An isotropic etch of the SiN_x layer was then performed to generate the undercut that defines the toroidal gaps of the coaxial structures. 6) A thin Ti layer (5 nm), used to improve the metal adhesion to the GaAs, and a thicker Au layer (50 nm) were deposited to form the central coaxial regions. After this metal deposition, a lift-off step using the sacrificial PMMA layer removed the Au everywhere except in the coaxial centers. 7) Next, deposition and etch-back steps were used to re-planarize the surface. A thick layer of photoresist (AZ-5214; 1.9-μm thick) was spun on the sample and etched back to expose the remaining SiN_x layer: The same O_2-plasma recipe for etching the BARC (step 4) was used to etch-back the resist and expose the underlying SiN_x layer. 8) The remaining SiN_x was removed by selective wet etching with buffered oxide etch (BOE) 6:1, leaving a PR filler surrounding the center dot and the toroidal regions. 9) A second Ti/Au-film was deposited to provide the outer webbing and a final PR lift-off completed the structure.

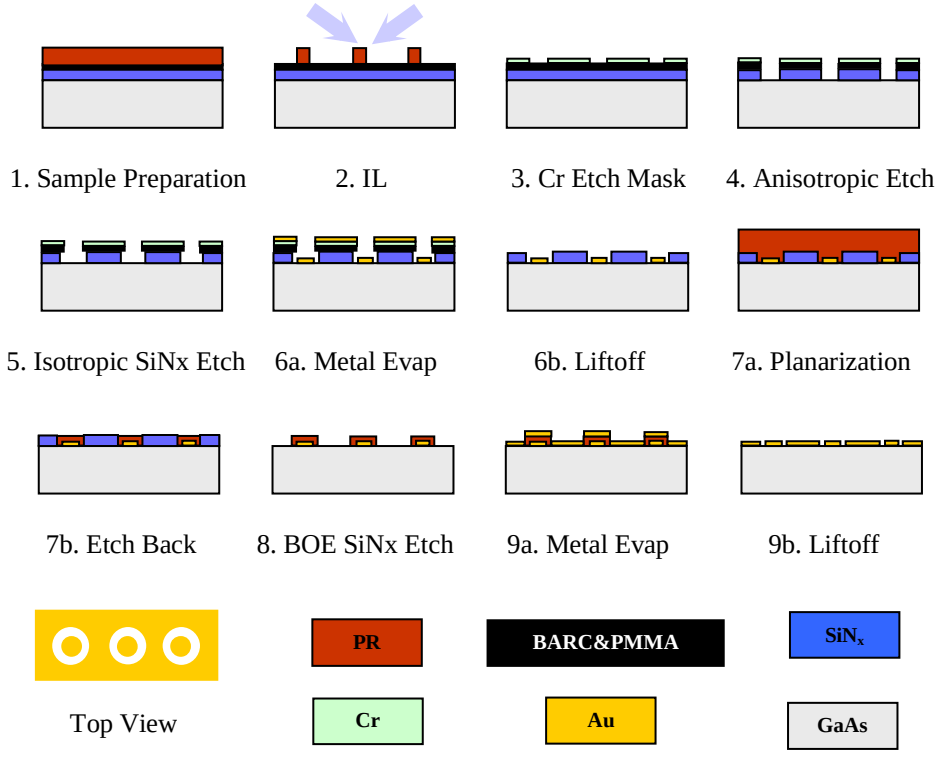

Fig. 1. Processing flow scheme (see text for detailed description).

#7338 - $15.00 USD
Received 3 May 2005; revised 27 May 2005; accepted 27 May 2005

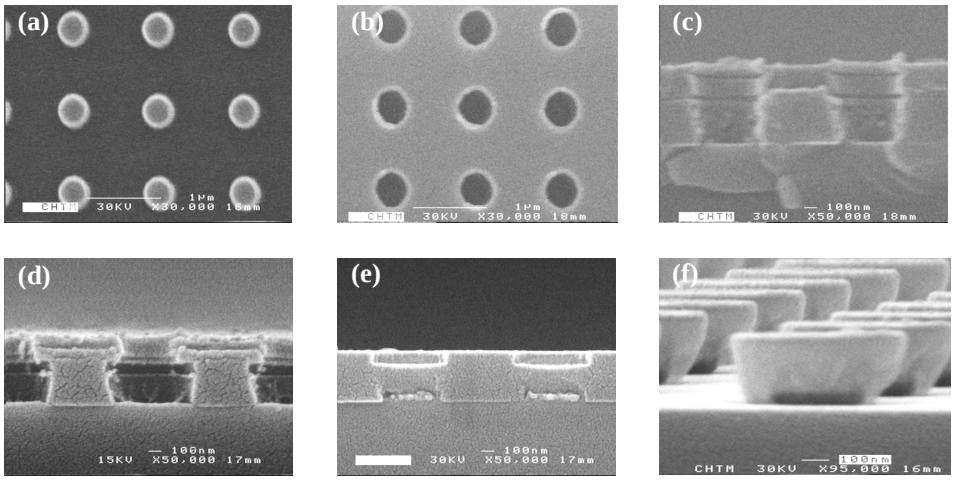

Fig. 2. SEM pictures of the critical steps for fabrication of annular metallic coaxial arrays: (a) Top view of PR post array after IL; (b) Top view of Cr etch mask; (c) Cross-section view after anisotropic etching, the layers from top to bottom are Cr, BARC, PMMA, SiN_x and GaAs substrate; (d) Cross-section view after isotropic etching of SiN_x, the undercut of the SiN_x defines the coaxial gap; (e) Cross-section view after planarization and etch back steps, the SiN_x layer is exposed and the PR fills the hole on top of the center Au dot; (f) Tilted-view of PR filler covering on top of the center Au dot (thin dark shadow dot in the picture) after BOE etch for removal of the SiN_x sacrificial layer.

The scanning electron micrographs (SEM) in Fig. 2 show the critical process steps. A subwavelength metallic hole array was also fabricated, in order to compare its optical properties with the annular metallic coaxial arrays. SEMs of the final hole array sample and all five coaxial samples are shown in Fig. 3.

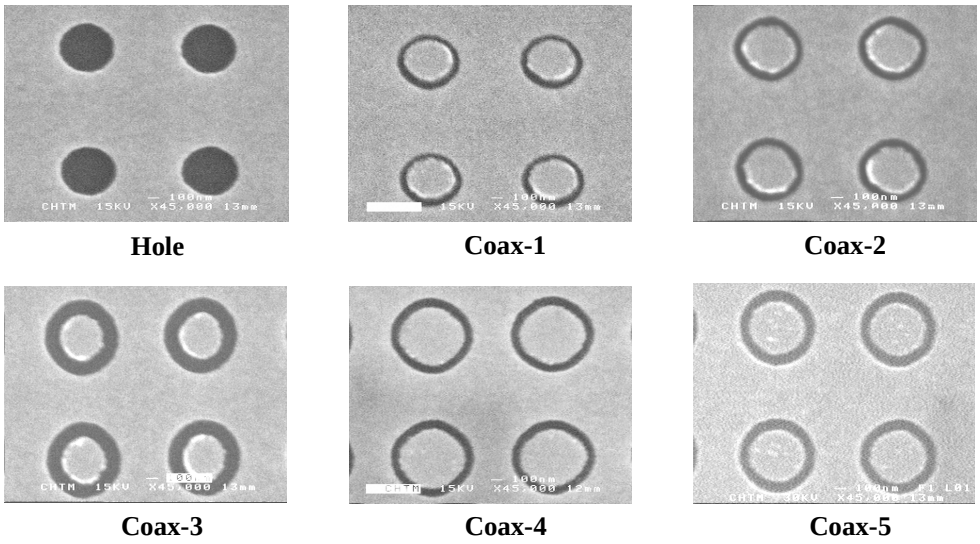

Fig. 3. SEM pictures of five different 1.12-μm pitch annular coaxial arrays and the hole array; structure dimensions are provided in Table I.

#7338 - $15.00 USD Received 3 May 2005; revised 27 May 2005; accepted 27 May 2005

3. Measurement and analysis

Transmission spectra were recorded using a Nicolet™ Fourier-transform infrared (FTIR) spectrometer with a KBr beam splitter (spectral range 11000 – 375 cm^{-1}) and a DTGS-KBr detector (spectral range 12500 – 350 cm^{-1}). Spectral transmission measurements were performed at normal incidence with an unpolarized, incoherent, white-light source. For the square symmetry of the pattern, the normal incidence transmission is polarization independent. All spectra were normalized to the transmission of an air background and the nanostructured coaxial array transmission is significantly larger than hole array transmission. For clarity, each coaxial array sample transmission spectrum has been offset by an additional 2% in Fig. 4 (the left vertical axis is for the hole array; the right vertical axis for the coax-5 sample). The transmission spectrum of a bare double-polished GaAs sample was measured as well. For the wavelength range of the measurement, the transmission of the substrate is approximately 53%, thus normalization of these spectra to that of a bare GaAs substrate essentially doubles the transmission results.

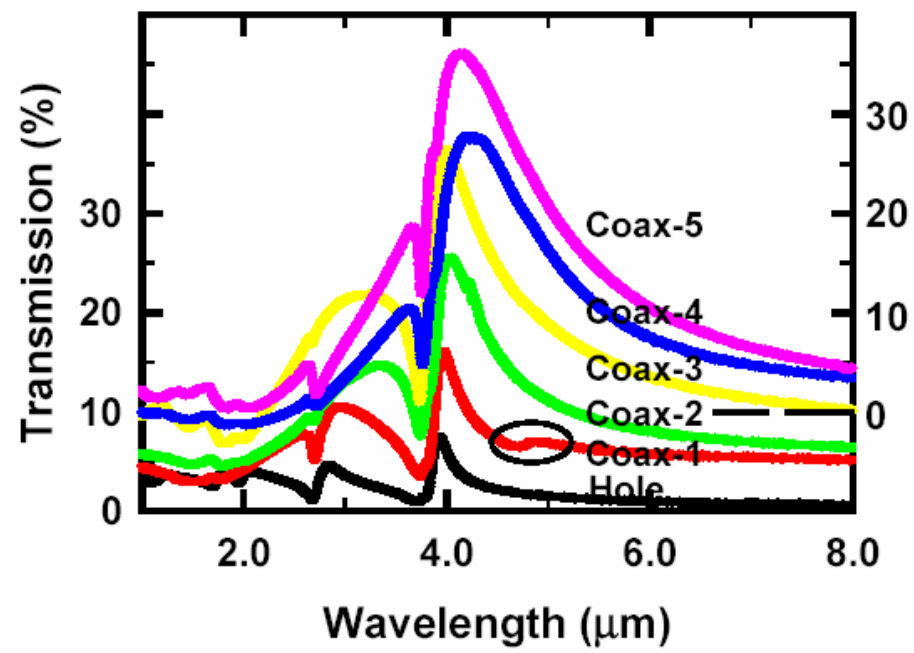

Fig. 4. Transmission spectra of different metallic coaxial and hole arrays. The individual spectra are each vertically offset by 2% for clarity. The left vertical axis is for the hole array, the right vertical axis for the coax-5 sample.

The geometric parameters of all of the samples are listed in Table I, along with a summary of the transmission spectra. All five of the coaxial array structures showed both an increase in the peak transmission and a shift of the peak to longer wavelengths compared to the hole array. For sample Coax-5, 36% transmission was observed at 4.15 μm. The fractional open area within each unit cell of the array was only 15%: an open annulus of width 102 nm and an inner radius of 248 nm (outer radius 350 nm) on a 1.12-μm period square array unit cell. For the 255-nm diameter hole array with a fractional open area of 16%, a peak transmission of only 7.5% was obtained at 3.93 μm. With a slightly smaller fractional open area, the coax-5 sample shows roughly five times higher peak transmission. The enhanced transmission and the peak shift are the results of the coupling between a localized mode, the coaxial TE_{11} mode supported by the coaxial unit cell, and the delocalized surface plasma wave modes of the metal film [11].

#7338 - $15.00 USD Received 3 May 2005; revised 27 May 2005; accepted 27 May 2005

Table I. Summary of sample dimensions and transmission results.

	a-Inner Radius (nm)	b-Outer Radius (nm)	Coax Gap (nm)	a + b (nm)	Peak (μm)	Opening Area (%)	Trans-mission (%)	T(%)/ A(%)
Hole	--	255	--	255	3.93	16	7.5	0.46
Coax-1	224	286	62	510	3.97	8	14.1	1.77
Coax-2	230	308	78	538	4.03	11	21.5	2.04
Coax-3	202	347	146	549	4.00	20	30.4	1.52
Coax-4	277	363	86	640	4.26	14	29.8	2.16
Coax-5	248	350	102	598	4.15	15	36.1	2.36

The dip in the hole transmission spectra at (~3.7 μm ~ $n_{GaAs}L$ where L is the array period) corresponds to the Wood's anomaly at the horizon for the first-order diffraction in the substrate. The peak of the hole-array sample transmission at 3.93 μm (just longer in wavelength than the Wood's anomaly feature) corresponds to coupling from a normal-incident photon to the surface plasma wave bound to the Au-GaAs surface. It is known that these two features are related parts of an asymmetric Fano-resonance lineshape [14]. Structure at this wavelength is evident in all of the coaxial array spectra as well. The structure around 2.7 μm corresponds to the same Wood's anomaly/SPW Fano resonance with a larger pitch grating corresponding to the diagonal of the square unit cell (~$n_{GaAs}L/\sqrt{2}$). All of the coaxial arrays show a dominant feature to longer wavelengths that is not present for the hole array and that has been previously identified [10, 11] as arising from the cutoff of the TE_{11} coaxial mode. The small peak around 4.87 μm for sample Coax-1, circled in Fig. 4, does not have counterparts on the other spectra. It is likely due to lifting the degeneracy of the coax TE_{11} mode, since the Au dot of sample Coax-1 is a little off-center as can be seen in Fig. 3. The structure around 4.2 μm on the transmission spectra of samples Coax-2 and Coax-5 is instrumental, due to atmospheric CO_2 absorption in the FTIR optical path.

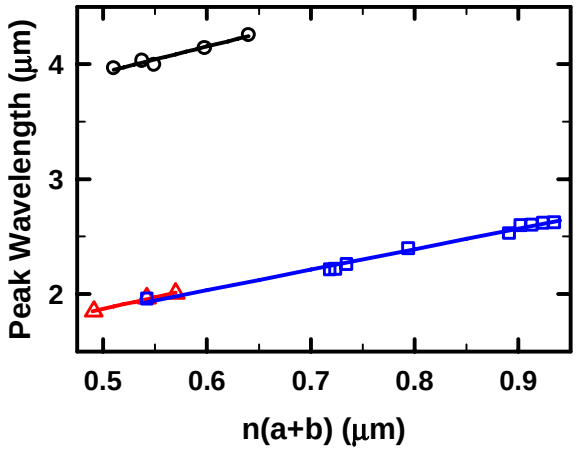

Fig. 5. Variation of transmission peak wavelength with coaxial geometry. n is the refractive index of the coax gap media. Date points of different coaxial samples from this paper where n = 1 is fixed (black circles); data points of different coax samples from ref. 11 where n = 1 (red triangles); and data points from ref. 11 where n varies and a+b is fixed (blue squares).

As expected for a TE_{11} mode [15], the peak transmission, corresponding to the cutoff wavelength [16] of an infinitely long coaxial transmission line, $\lambda_{cutoff} = 1.873\pi n(a+b)/2 \sim 3n(a+b)$,

#7338 - $15.00 USD Received 3 May 2005; revised 27 May 2005; accepted 27 May 2005

is linearly dependent on the refractive index of the coax gap medium and on the sum of the inner and outer radii, shifting to longer wavelength as these values increase as shown in Fig. 5, where the data from this paper and from data reference 11 are summarized. The transmission peaks clearly reflect the coaxial geometry. All of the data sets have the same slope ~ $2n(a+b)$. However, the curves have different y-axis intercepts on the different substrates, namely GaAs (n ~ 3.4) and SiO_2 (n ~ 1.47). Since the coaxial structure is $<<\lambda$ in the vertical direction, fringing effects are expected to be significant in these measurements and may account for these deviations from the simple cutoff formula. Further experimental and simulation studies are underway to find a general description of the coaxial peak resonance position.

An RCWA simulation (not shown) has been used in investigate the impact of a change in the array period on the coaxial resonance position, which is essentially independent of the array period as expected. However, the strength of the resonance, and hence the transmission, shows a clear correlation with the relative positions of the SP and TE_{11} resonances. Simulation gives the best value of the figure of merit, transmission divided by the open area, when the coaxial resonance overlaps with the (0, 1) SP (GaAs-metal) resonance.

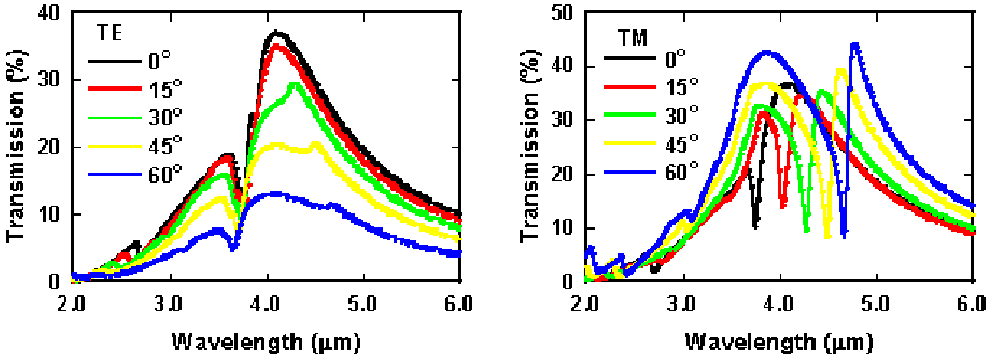

Fig. 6. Transmission spectral dependence on incident angle for TE (left) and TM (right) polarized light for sample coax-5.

At normal incidence, the transmission is independent of polarization for this square symmetric pattern. The transmission spectra of sample Coax-5 was investigated for angles of incidence between 0^o and 60° for both TE and TM polarizations. A gold wire-grid polarizer, effective only for wavelengths longer than 2 μm, was used. Away from normal incidence, there is a strong difference between the TM and TE transmission spectra. For TM polarized light, as the incident angle increases the transmission peaks evolve dramatically as the delocalized SP mode shifts to longer wavelength passing through the localized TE_{11} mode resonance. The asymmetric Fano line shapes clearly show coupling between these modes. In contrast, no strong features appear in the TE polarization measurement since the SP coupling is independent of angle for this polarization. Fig. 6 shows several spectra at different angles, the dispersion curve extracted from the photon energy of transmission peaks of TM polarization light shows similar behavior to that reported in ref. 11 for a shorter wavelength resonance on a glass substrate. The spectra for TE polarized light show a gradual shift towards lower transmission at higher angles, but no new features appear. (The weak features evident at 4.2, 4.5 and 4.8 mm for the 30°, 45° and 60° TE curves follow the strong features in the TM spectra and are likely due to a small polarization misalignment.)

4. Conclusion

Interferometric lithography has been used to fabricate large-area, annular-coaxial, metal, thin-film arrays on a high refractive-index semiconductor material. A fivefold enhancement in the

#7338 - $15.00 USD Received 3 May 2005; revised 27 May 2005; accepted 27 May 2005

transmission as compared to a simple hole array with roughly the same fractional open area has been demonstrated. This is dramatic difference from the result for a low-index (SiO_2) substrate where the comparable enhancement was only ~ 1.9. Design rules for shifting the wavelength depending on the coaxial dimensions and the dielectric properties of the substrate materials and the material inside the coaxial toroid are elucidated, providing a design approach to shifting the resonance wavelength. Applications of these nanophotonic structures to nonlinear optics and infrared sensing are under investigation.

Acknowledgments

This work was supported by the U.S. Army Research Office under the MURI program in Deep Subwavelength Optical Nanolithography and by the Defense Advanced Research Projects Agency. Facilities of the NSF NNIN were used in the fabrication.

#7338 - $15.00 USD Received 3 May 2005; revised 27 May 2005; accepted 27 May 2005